Improved battery storage systems modeling for predictive energy management applications

Ricardo Silva, Clara Gouveia, Leonel Carvalho, Jorge Pereira
Institute for Systems and Computer Engineering (*INESC TEC)*
Porto, Portugal
ricardo.emanuel@inesctec.pt, clara.s.gouveia@inesctec.pt, leonel.m.carvalho@inesctec.pt, jorge.c.pereira@inesctec.pt

2022 IEEE PES Innovative Smart Grid Technologies Conference Europe (ISGT-Europe) | 978-1-6654-8032-1/22/$31.00 ©2022 IEEE | DOI: 10.1109/ISGT-Europe54678.2022.9960620

***Abstract*— This paper presents a model predictive control (MPC) framework for battery energy storage systems (BESS) management considering models for battery degradation, system efficiency and V-I characteristics. The optimization framework has been tested for microgrids with different renewable generation and load mix considering several operation strategies. A comparison for one-year simulations between the proposed model and a naïve BESS model, show an increase in computation times that still allows the application of the framework for real-time control. Furthermore, a trade-off between financial revenue and reduced BESS degradation was evaluated for the yearly simulation, considering the degradation model proposed. Results show that a conservative BESS usage strategy can have a high impact on the asset's lifetime and on the expected system revenues, depending on factors such as the objective function and the degradation threshold considered.**

Keywords— battery degradation, battery energy storage systems, linear model, microgrid, model predictive control.

NOMENCLATURE

Indices and sets

$t \in T$	Set of time intervals within the optimization horizon.
$s \in S$	Set of piecewise segments approximating the BESS efficiency curve.

Parameters

$\overline{\varepsilon}^b(.), \underline{\varepsilon}^b(.)$	BESS dynamic maximum/minimum energy content [Wh].
$\overline{E}^b, \underline{E}^b$	BESS absolute maximum/minimum energy content [Wh].
$\hat{V}^{N,+}, \hat{V}^{N,-}$	Nominal charge and discharge voltage [V]
$\widehat{m}^{b,+}, \hat{o}^{b,+}$	Line parameters for dynamic energy content linearization when charging
$\widehat{m}^{b,-}, \hat{o}^{b,-}$	Line parameters for dynamic energy content linearization when discharging
$\widehat{m}^{\eta,+}, \hat{o}^{\eta,+}$	Line parameters for inverter efficiency linearization when charging
$\widehat{m}^{\eta,-}, \hat{o}^{\eta,-}$	Line parameters for inverter efficiency linearization when discharging
$\overline{P}^{b,+}, \overline{P}^{b,-}$	BESS charge/discharge power rate limit [W].
$\hat{\eta}^{b,+}, \hat{\eta}^{b,-}$	BESS charge/discharge efficiency.
$\hat{E}^{b,N}$	BESS nominal capacity [Wh]
$\widehat{m}^{deg}$	Slope of degradation curve's linearization
$\overline{E}^{deg}$	Limit for the BESS daily degradation [Wh]
$\hat{\lambda}_t^{mk}, \hat{\lambda}_t^{fi}$	Forecasted market prices/feed-in tariffs for t [€/Wh].
$\hat{\lambda}_t^L$	Cost of load curtailment for t [€/Wh].
$\hat{P}_t^G$	Forecasted RES generation during t [W].
$\hat{P}_t^L$	Forecasted load demand during t [W].
$\overline{P}^{G,cut}$	Maximum curtailable RES capacity [W].
$\overline{P}^{AC,+}, \overline{P}^{AC,-}$	Inverter charge/discharge power rate limit [W].
Δt	Length of the optimization time step [h].
$\hat{E}^{deg,T^1}$	Degradation observed in previous steps of current day [Wh]
$\overline{P}_s^{b,+}, \overline{P}_s^{b,-}$	BESS maximum charge/discharge power rate limit for segment s [W].
$\underline{P}_s^{b,+}, \underline{P}_s^{b,-}$	BESS minimum charge/discharge power rate limit for segment s [W].

Variables

$p_t^{b,+}, p_t^{b,-}$	BESS charge/discharge setpoint during t [W].
e_t^{deg}	Battery's degraded capacity at the end of t [Wh].
p_t^{abs}, p_t^{inj}	Absorption/injection setpoint at the PCC during t [W].
$p_t^{L,cut}$	Load curtailment setpoint during t [W].
$\Delta e_t^+, \Delta e_t^-$	Positive/negative energy imbalance at t [Wh].
$p_t^{G,cut}$	RES curtailment setpoint during t [W].
e_t^b	BESS energy content at the end of t [Wh].
$\delta_t^{PCC}, \delta_t^b$	Binary variables to avoid simultaneous inverse power flows during t.
e_t^{DA}, e_t^{PCC}	Energy scheduled/effectively injected (< 0)/ absorbed (≥ 0) at the PCC, during t [W].
Δe_t^b	Change in BESS energy content in t as a result of the applied power $p_t^{b,+/-}$ [Wh].
$z_t^{b,+}, z_t^{b,-}$	BESS charge/discharge setpoint (DC side) in the 1st line segment, during t [W].
$p_{t,s}^{b,+}, p_{t,s}^{b,-}$	BESS charge/discharge setpoint (AC side) in the sth line segment, during t [W].
$\delta_{t,s}^{b,+}, \delta_{t,s}^{b,-}$	Binary variable for enabling BESS charge/discharge within segment s, during t.

I. INTRODUCTION

The operation of renewable-based power systems increasingly relies on the optimal exploitation of battery energy storage systems (BESS) and flexible loads. Optimal scheduling of BESS has been widely covered in literature, integrated for example in microgrids, energy communities and renewable power generation plants. The use of model predictive control (MPC) as, for example, showed in [1], presents an adequate framework for real-time, on-line scheduling of BESS, being able to compensate at each time step for real-time disturbances or forecast errors.

In most cases, a simplified BESS modelling approach is considered, adopting constant battery charging/discharging powers and efficiency. This naïve model can be found on most optimal BESS control strategies, as highlighted in [2]. In [3], the authors have tested the impact of modelling battery dynamics and electrochemical degradation in the optimal control strategy of BESS, demonstrating that a simplified model could, although, lead to an erroneous techno-economic performance assessment. Also, [4] and [5] analyse the impact of the operation strategy in BESS lifetime selected, that in most dispatch problems is neglected.

This paper proposes an enhanced BESS modelling approach for an MPC framework, that aims at balancing computational tractability with accuracy, based on three fundamental characteristics: battery degradation, system efficiency and V-I characteristics. To the extent of our knowledge, no other work has proposed such a complete and tractable model, applicable to Mixed Integer Linear Programming (MILP) formulations. Considering this framework, an analysis is performed over the impact of adopting distinct BESS usage strategies on different systems and objective functions.

II. BESS LINEAR MODEL

A linear model of BESS is considered, specifically designed for Li-ion technologies, and focused on three fundamental characteristics: V-I characteristics, system efficiency and degradation.

A. V-I characteristics

We adapted the model presented at [6](recently described as the C/L/C model at [7]), that adds to the MILP formulation the possibility to adjust the battery energy content limits as a function of the power setpoints' magnitude imposed at each time step. The definition of dynamic energy content limits, $\underline{\varepsilon}^b(.)$ and $\overline{\varepsilon}^b(.)$, stems from the fact that the battery cannot charge or discharge completely (i.e., reach the absolute, static, energy content limits, $\underline{E}^b$ and $\overline{E}^b$) when subjected to high charge and discharge currents, respectively, due to the voltage spike/drop associated. These limits represent the energy content of the battery when its voltage limits are reached, being more restrictive when higher discharge or charge currents are applied, respectively. We establish therefore the chain of magnitude $\underline{E}^b \leq \underline{\varepsilon}^b\left(\frac{p_t^b}{\hat{V}^{N,-}}\right) \leq e_t^b \leq \overline{\varepsilon}^b\left(\frac{p_t^b}{\hat{V}^{N,+}}\right) \leq \overline{E}^b$. The definition of the BESS nominal charge ($\hat{V}^{N,+}$) and discharge ($\hat{V}^{N,-}$) voltages, along with the parameters for $\underline{\varepsilon}^b(.)$ and $\overline{\varepsilon}^b(.)$ linearization (slopes $\widehat{m}^{b,+/-}$ and origins $\hat{o}^{b,+/-}$) can be achieved through a combination of the manufacturer's information and relatively simple tests, whose methodology can be consulted at [6].

B. System efficiency

BESS inverters' efficiency is nonlinear for small output powers (see Fig. 1). A 2-step piecewise model was defined to linearly approximate the charge and discharge efficiency curves for output powers below and above an empirical threshold (10%) of the inverter's rated power. The computational burden of considering additional steps for higher output powers does not justify the decrease of the approximation error. The parameters for the first line segment (slopes $\widehat{m}^{\eta,+/-}$ and origins $\hat{o}^{\eta,+/-}$), are obtained by performing a least squares approximation of the available test values below the rated power's threshold. In order to embed this model in the MILP, the line parameters for charging and discharging must be obtained for different curves than the one depicted in Fig. 1: the line's abscissa corresponding to the rated power intervals $]0, 0.1 \times \overline{P}^{b,+}]$ and $]0, 0.1 \times \overline{P}^{b,-}]$, respectively; the line's ordinates to the DC-side power setpoints from the experimental trials, $P^{b,+} \times \hat{\eta}^{b,+}(P^{b,+})$ and $\frac{P^{b,-}}{\hat{\eta}^{b,-}(P^{b,-})}$, respectively. This linear approach converts an AC to a DC-side power setpoint, avoiding a non-linearity that would result from multiplying the calculated efficiencies by the AC-side power setpoints. The second segment is obtained by averaging the observed efficiencies for values above the 10% threshold. This segment is then extended backwards until the intersection point with the first one, avoiding possible large discontinuities in the vicinity of the threshold. Equation (1) is used to obtain this new power threshold between segments, either for charging or discharging.

$$\overline{P}_{s=1}^{b,+/-} = \underline{P}_{s=2}^{b+/-} = \frac{\left(\hat{\eta}^{b+/-} \times 0.1 \times \overline{P}^{b,+/-} - \hat{o}^{\eta,+/-}\right)}{\hat{o}^{\eta,+/-}}. \tag{1}$$

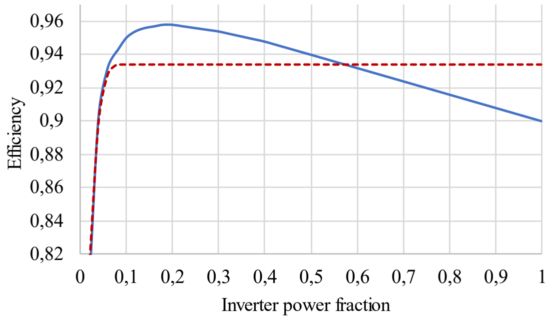

Fig. 1. Typical inverter's charge effecency curve (adapted from [8]). The two-step piecewise linearization proposed is depicted in dashed red.

C. Degradation

BESS degradation can be accounted for by limiting its total allowed value within the optimization's horizon, based on the discharging cycles imposed. Starting from the battery's degradation curve provided by the manufacturer (Fig. 2), which relates the depth of discharge (DOD) with the total number of cycles until the end-of-life (EOL) criterion is met (e.g., 70% of the initial battery's capacity $\hat{E}^{b,N}$) a relationship is established between DOD and the corresponding percentage of cycle life loss (i.e., loss of storage capacity; see Fig. 3). The conversion between curves is performed by applying (2). The cycle life loss curve is linearized by a least squares' approximation, forcing it to intersect the origin. The line's slope $\widehat{m}^{deg}$ is used to estimate the degradation caused by each discharge cycle using (3). The EOL criterion can then be used to define a maximum daily capacity degradation value $\overline{E}^{deg}$, using (4).

$$Cycle\ life\ loss\ (DOD) = \frac{100-EOL}{Number\ of\ cycles(DOD)} \tag{2}$$

$$e_t^{deg} = \widehat{m}^{deg}\ \frac{p_t^-}{\hat{\eta}^{b,-}},\ e_t^{deg} \in \mathbb{R}_0^+ \tag{3}$$

$$\overline{E}^{deg} = \frac{(100-EOL)\hat{E}^{b,N}}{100 \times 365}. \tag{4}$$

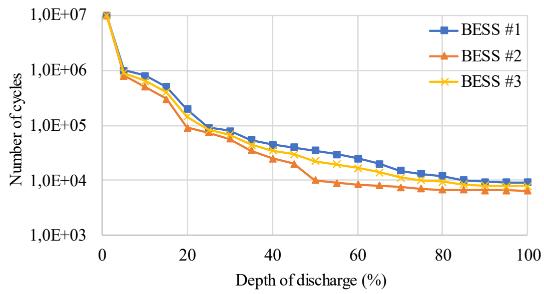

Fig. 2. Typical manufacturer's degradation curves for Li-ion batteries.

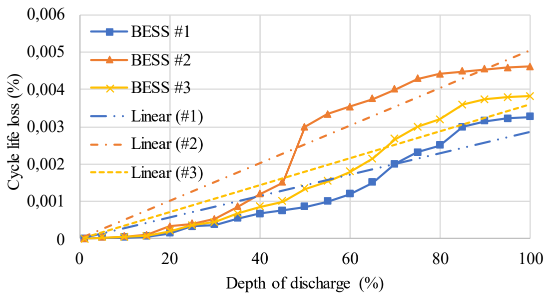

Fig. 3. Cycle life loss curves resulting from adapting the curves in Fig. 2. A depiction of each curve's linearization is provided as dashed lines.

III. Predictive Energy Management Algorithm

This section describes the proposed optimal operation scheduling algorithm for a microgrid integrating BESS, different types of renewable energy sources' (RES) generation and load assets (flexible and non-controllable). The algorithm is aimed at running in real-time, based on an MPC framework. The provided outputs include the BESS active power schedules and setpoints for renewable generation and load curtailment, when required. For the sake of simplicity, the equations presented assume a single aggregated representation per asset type (renewable generation, load demand and BESS) but can easily be adapted to consider multiple assets per type.

The problem was formulated as a MILP with two optional objective functions: price arbitrage (OF1) described in (5) and minimizing energy deviations (OF2) described in (6) from a pre-defined schedule (e.g., resulting from market clearing or central dispatch).

$$Min \sum_{t\in T}\left(p_t^{abs}\hat{\lambda}_t^{mk} - p_t^{inj}\hat{\lambda}_t^{fi} + p_t^{L,cut}\hat{\lambda}^{L,cut}\right)\Delta t \quad (5)$$

$$Min \sum_{t\in T}\left(\Delta e_t^- + \Delta e_t^+ + p_t^{L,cut}\hat{\lambda}^{L,cut}\right) \quad (6)$$

Note that when $\Delta e_t^{\Delta,-} > 0$ there is a deficit of injected energy and if $\Delta e_t^{\Delta,+} > 0$, there is an excess of injected energy regarding the day-ahead scheduled value for time step t. Both deviations are penalized in (6). A load curtailment cost ($\hat{\lambda}^{L,cut}$) is also defined, typically high to ensure its use as a last resort.

The constraints applied in the general formulation include: (7), an equilibrium equation; (8) to limit, when applicable, RES curtailment; (9) and (10) to limit power throughput rates at the BESS; (11) to update the energy content of the BESS between steps; and (12) to bound that energy content within the battery's limits. If the objective function chosen is (6), then (13) and (14) must also be added to calculate the energy imbalances.

$$p_t^{abs} - p_t^{inj} = p_t^{b,+} - p_t^{b,-} - \hat{P}_t^G + p_t^{G,cut} + \hat{P}_t^L - p_t^{L,cut},$$
$$\forall\, t \in T, p_t^{abs}, p_t^{inj} \in \mathbb{R}_0^+ \quad (7)$$

$$p_t^{G,cut} \le \overline{P}^{G,cut}, \ \forall\, t \in T \quad (8)$$

$$0 \le p_t^{b,+} \le \overline{P}^{AC,+}\delta_t^b, \ \forall\, t \in T \quad (9)$$

$$0 \le p_t^{b,-} \le \overline{P}^{AC,-}(1-\delta_t^b), \ \forall\, t \in T \quad (10)$$

$$e_t^b = e_{t-1}^b + \left(p_t^{b,+}\hat{\eta}^{b,+} - \frac{p_t^{b,-}}{\hat{\eta}^{b,-}}\right)\Delta t, \ t \in T \quad (11)$$

$$\underline{E}^b \le e_t^b \le \overline{E}^b \quad (12)$$

$$e_t^{PCC}\frac{1}{\Delta t} = p_t^{abs} + p_t^{inj}, \ \forall\, t \in T \quad (13)$$

$$\Delta e_t^- - \Delta e_t^+ = e_t^{PCC} + e_t^{DA}, \ \forall\, t \in T, \Delta e_t^-, \Delta e_t^+ \in \mathbb{R}_0^+ \quad (14)$$

The MILP general formulation further includes the possibility to dispatch curtailable loads, introducing restrictions related to the maximum downtime ($\hat{T}^{MD}$) followed by a minimum uptime ($\hat{T}^{mU}$). Rebound effect is not considered.

A. Considering a limit to BESS daily degradation

To consider a daily limit to BESS degradation, as explained in section II.C., (15) must be included in the MILP formulation. Since the algorithm was designed to be implemented within an MPC framework, if $T > 12h$, the optimization horizon of MILPs at a certain iteration of the MPC will encompass not only steps within the day being optimized ($t \in T^1$), but also steps of the next day ($t \in T^2$). Please note that $\{T^1, T^2\} = T$ and that if $T \le 12h \Rightarrow T^1 = T$. e_t^{deg} needs to be reset for $t \in T^2$ which is achieved by implementing (16). Note that the BESS degradation since t=1, $\hat{E}^{deg,T^1}$, is given by previous iterations of the MPC.

$$\sum_t^{T^1} e_t^{deg} \le \overline{E}^{deg} - \hat{E}^{deg,T^1} \quad (15)$$

$$\sum_t^{T^2} e_t^{deg} \le \overline{E}^{deg} \quad (16)$$

B. Considering V-I characteristics

To consider variable energy content limits, (12) must be replaced by (17).

$$\widehat{m}^{b,-}\frac{p_t^{b,-}}{\hat{\eta}^{b,-}} + \hat{o}^{b,-} \le e_t^b \le \widehat{m}^{b,+}p_t^{b,+}\hat{\eta}^{b,+} + \hat{o}^{b,+}, \ \forall\, t \in T$$
$$(17)$$

C. Considering a linear approximation to the inverter's efficiency curve

First, the terms $p_t^{b,+}\hat{\eta}^{b,+}$ and $\frac{p_t^{b,-}}{\hat{\eta}^{b,-}}$ at (11) and (28) must be substituted by $Z_t^{b,+} + P_{b,t,2}^+\hat{\eta}_b^+$ and $Z_t^{b,-} + \frac{P_{b,t,2}^-}{\hat{\eta}_b^-}$, respectively. Next, (9) and (10) must be substituted by (18) and (19), respectively, and considering S = [1, 2].

$$\underline{P}_s^{b,+}\delta_{t,s}^{b,+} \le p_{t,s}^{b,+} \le \overline{P}_s^{b,+}\delta_{t,s}^{b,+}, \ \forall\, t \in T, s \in S \quad (18)$$

$$\underline{P}_s^{b,-}\delta_{t,s}^{b,-} \leq p_{t,s}^{b,-} \leq \overline{P}_s^{b,-}\delta_{t,s}^{b,-},\ \forall\, t \in T, s \in S \quad 19$$

Additionally, the following constraints must be considered:

$$z_t^{b,+} = \widehat{m}^{\eta,+} p_{t,1}^{b,+} + \hat{o}^{\eta,+}\delta_{t,1}^{b,+},\ \forall\, t \in T, s \in S \quad (20)$$

$$z_t^{b,-} = \widehat{m}^{\eta,-} p_{t,1}^{b,-} + \hat{o}^{\eta,-}\delta_{t,1}^{b,-},\ \forall\, t \in T, s \in S \quad (21)$$

$$\textstyle\sum_s\left(\delta_{t,s}^{b,+} + \delta_{t,s}^{b,-}\right) \leq 1,\ \forall\, t \in T, s \in S. \quad (22)$$

Note that (20) and (21), for a constant segment, must be defined as $p_{t,s}^{b,+/-} = \hat{o}^{\eta,+/-}\delta_{t,s}^{b,+/-}$, respectively, since $\widehat{m}^{\eta,+/-} = 0$.

IV. Case Study and Results

The algorithms were implemented in Python, using the linear programming modeler puLP [9] and the default COIN-OR Branch-and-Cut solver [10] setting the mipgap to 1E-3. The performance tests were conducted on a Laptop PC with AMD® Ryzen® CPU 5 PRO 4650U @2.10 GHz and a 16GB RAM.

The MG considered in the studies is composed of a total of 10 MWp of RES and a 5 MWh BESS. For studying the impact of including battery degradation limits, we considered the BESS desired lifetime to be 10 years and EOL = 70%, which leads to a daily maximum degradation $\overline{E}^{deg} = 17\ Wh$. The MG has a peak demand of 10 MVA, of which 25% is curtailable. For this simulation, we considered that all assets remain active throughout the year, i.e., no maintenance is defined.

The simulations were performed over four scenarios for comparing a BESS basic model with the proposed model along two different objective functions. One year PV and load forecasts were adopted from real measurements [11] and [12]. Historical spot market prices of MIBEL [13] were used and feed-in tariffs were estimated as a variable, inferior percentage of those prices. When minimizing energy deviations (OF2), day-ahead bids were simulated by adding gaussian white noise to the forecasted net load so that the mean absolute percentage error (MAPE) between day-ahead bids and forecasts was roughly 10%.

A. BESS daily energy dispatch

Fig. 4 shows the net load of the microgrid and the prices and tariffs applicable during a randomly selected day. Fig. 5 shows the results of the microgrid dispatch problem for that day. In this case BESS degradation was not limited and only BESS V-I characteristics and inverter efficiency were considered. BESS usage follows the market signals, and the difference between using a naïve and the enhanced proposed model is highlighted.

As shown in Fig. 5, adopting the proposed BESS model leads to small differences in the energy dispatch strategy, when compared to the simplified model. This occurs since the model proposed updates the charging limits as a function of the power setpoints' defined by the optimization problem. For example, at t=4, t=10 and t=15 maximum charging power is limited, changing the scheduling strategy. This leads to a small reduction of microgrid operation costs, from -826,44€ for the naïve model to -819,23€ for the enhanced model.

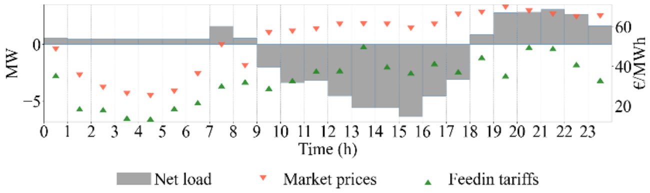

Fig. 4. Example the net load, market prices and feedin tariffs considered, for a day with particular high renewables' generation.

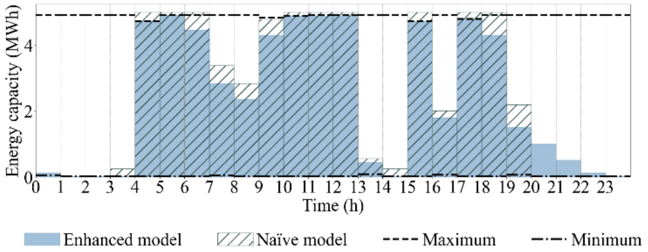

Fig. 5. Example of a single BESS dispatch on a microgrid context uder OF1 for the day depicted at Fig. 4.

B. Impact of battery degradation in BESS dispatch strategy

The impact of considering battery degradation in the BESS scheduling problem was tested for both objective functions. The results of simulating the first year of usage with a 1h step, are summarized in Table I. Considering the energy arbitrage strategy (OF1) there is a reduction on expected revenues of 27%, linked to a decrease in BESS degradation of 19%. There is a clear trade-off between liquid profitability and an increased BESS lifetime, which we can argue to accentuate with the degree of mismatch between generation and consumption profiles or the inadequacy of the BESS installed. Another factor that can have the reverse effect on that trade-off is the adequacy of the maximum daily degradation threshold to the objective function. By analysing the results for OF2 (minimizing energy deviations), we found no differences between both strategies. Given the low error between day-ahead bids and forecasts, the need to use the flexibility of the BESS is reduced, which is supported by its average daily usage generating a degradation (6 Wh) less than the maximum of 17 Wh. Clearly the daily degradation restriction, defined as it was, had no impact on this scenario.

TABLE I. Difference in total and average objective function and degradation values between BESS usage strategies. Note: negative vaues for OF1 represent a profit.

Obj. Func.	Strategy	Obj. Func. Value		Degradation (kWh)	
		Total	Average	Total	Average
OF1	conservative	-6982 €	-19 €	138	0,38
	unconstrained	-9599 €	-26 €	170	0,47
OF2	conservative	145 MWh	0.40 MWh	2	0,005
	unconstrained	145 MWh	0.40 MWh	2	0,005

C. BESS model tractability and computational efficiency

A sensitivity analysis was carried out for the algorithms' performance and computational efficiency. Table II summarizes the average time required for the MILPs to reach an optimal solution for the 4 different scenarios over the year. Generally, the proposed model leads to an increase in the average optimization time, as expected. Nonetheless, the times presented are adequate for real-time applications relying on non-commercial solvers, thus enabling the implementation of an MPC framework.

TABLE II. AVERAGE OPTIMIZATION TIMES FOR DIFFERENT SCENARIOS.

BESS Model	Obj. Func.	Time (average)
Enhanced	OF1	3,212 s
	OF2	0,387 s
Naïve	OF1	0,157 s
	OF2	0,175 s

Fig. 5 shows the impact of the selected time horizon and timestep in the computational time, when considering the enhanced BESS model, on systems with increasing size. For this purpose, a microgrid with 10 BESS, 10 RES plants and 10 load assets, 50% of which are curtailable, were defined. A day in the dataset with high generation and consumption fluctuations was selected for a series of trial runs on both systems, including the two objective functions and different horizons (6h, 12h and 24h), and timesteps (5', 15' and 60'). To comply with the smaller steps, the data was resampled (original load forecasts had a 30' step while generation, market and feed-in data had a 1h step). Three independent runs were performed for each combination to determine an average performance. Again, even with more complex systems, we observed that the model is suited for real-time applications.

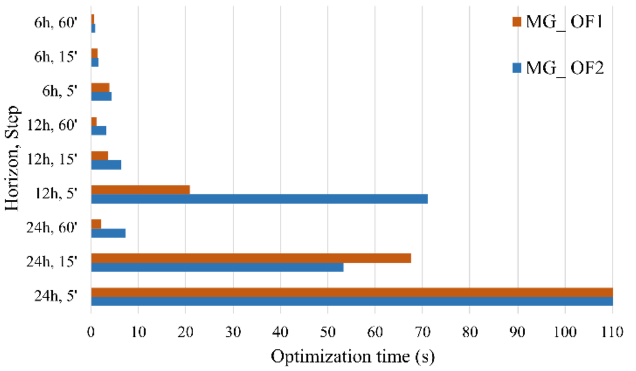

Fig. 6. Optimization time comparison between different objective function, horizon and step scenarios.

V. CONCLUSIONS

This work presented an optimization framework for real-time operation of microgrids, considering a linear model for BESS. The BESS model proposed is more accurate than widely used naïve models, considering VI-characteristics, system efficiency and degradation estimation and the results have demonstrated its tractability, ensuring its adequacy for real-time applications. The following assumptions are considered: energy is estimated assuming an idle state of the BESS, with constant voltage and BESS parameters namely its' degradation dynamics and energy content are considered constant throughout the optimization horizon (6-24h). In online operation they should be updated with BMS information regarding the battery State of Health (SoH) and total capacity estimation.

The simulations where BESS usage was constrained by a daily degradation limit highlighted the influence of 1) the adequacy of the installed capacities to the configured system; 2) the restrictiveness to be imposed on the daily degradation, and 3) the cost attributed to BESS degradation, whose definition resides outside the scope of this work. In practical applications, we recommend the BESS degradation curve to be updated from time to time. Further tests with real BESS need to be performed to identify the periodicity of such updates.

Finally, the simulation times obtained with non-commercial solvers allow to infer that the model presented is well suited for real-time operation of either system. There is the possibility of considering multiple asset types, thus resulting in an increased system complexity, without significantly impacting the simulation time, enabling the extension of the model to the MPC framework. For time steps smaller than 60 minutes, operation times can be further reduced with more powerful solvers.

ACKNOWLEDGMENTS

This work is financed by the ERDF - European Regional Development Fund, through the Operational Programme for Competitiveness and Internationalisation - COMPETE 2020 Programme under the Portugal 2020 Partnership Agreement, within project BATERIAS 2030, reference POCI-01-0247-FEDER-046109.

REFERENCES

[1] B. Heymann, J. F. Bonnans, P. Martinon, F. J. Silva, F. Lanas, and G. Jiménez-Estévez, "Continuous optimal control approaches to microgrid energy management," Energy Syst, vol. 9, no. 1, pp. 59–77, Feb. 2018, doi: 10.1007/s12667-016-0228-2.

[2] M. A. Hannan et al., "Battery energy-storage system: A review of technologies, optimization objectives, constraints, approaches, and outstanding issues," Journal of Energy Storage, vol. 42, p. 103023, Oct. 2021, doi: 10.1016/j.est.2021.103023.

[3] Y. Li and J. Wu, 'Optimum Integration of Solar Energy With Battery Energy Storage Systems', *IEEE Transactions on Engineering Management*, pp. 1–11, 2020, doi: 10.1109/TEM.2020.2971246.

[4] R. C. Guerrero, M. Angelo, and A. Pedrasa, 'An MILP-Based Model for Hybrid Renewable Energy System Planning Considering Equipment Degradation and Battery Lifetime', in *2019 IEEE 2nd International Conference on Power and Energy Applications (ICPEA)*, Apr. 2019, pp. 207–211. doi: 10.1109/ICPEA.2019.8818521.

[5] J. M. Reniers, G. Mulder, S. Ober-Blöbaum, and D. A. Howey, "Improving optimal control of grid-connected lithium-ion batteries through more accurate battery and degradation modelling," Journal of Power Sources, vol. 379, pp. 91–102, Mar. 2018, doi: 10.1016/j.jpowsour.2018.01.004.

[6] F. Kazhamiaka, C. Rosenberg, S. Keshav, and K.-H. Pettinger, "Li-ion storage models for energy system optimization: the accuracy-tractability tradeoff," Jun. 2016, pp. 1–12. doi: 10.1145/2934328.2934345.

[7] F. Kazhamiaka, C. Rosenberg, and S. Keshav, "Tractable lithium-ion storage models for optimizing energy systems," Energy Informatics, vol. 2, no. 1, p. 4, May 2019, doi: 10.1186/s42162-019-0070-6.

[8] J. Solano, "Energy And Economic Optimization Of Pv Hybrid Systems To Supply Buildings Hvac Demand: Battery Modeling And Control Strategies," 2018. doi: 10.20868/UPM.thesis.50457.

[9] pulp. COIN-OR Foundation, 2021. Accessed: Sep. 08, 2021. [Online]. Available: https://github.com/coin-or/pulp

[10] Cbc. COIN-OR Foundation, 2021. Accessed: Sep. 08, 2021. [Online]. Available: https://github.com/coin-or/Cbc

[11] G. P. Monteiro, A. I. Palmero-Marrero, C. Moreira, and A. C. Oliveira, "Evaluation of the performance of a photovoltaic power plant installed in a building in the north of Portugal," Energy Procedia, vol. 153, pp. 42–47, Oct. 2018, doi: 10.1016/j.egypro.2018.10.033.

[12] "SmartMeter Energy Consumption Data in London Households - London Datastore." https://data.london.gov.uk/dataset/smartmeter-energy-use-data-in-london-households (accessed Sep. 30, 2021).

[13] "SIMEE - Daily and Intraday - Prices." https://www.mercado.ren.pt/EN/Electr/MarketInfo/MarketResults/OMIE/Pages/Prices.aspx (accessed Sep. 08, 2021).